

Reverse Engineering Used to Profile a Gerotor Pump Rotor

Nicușor Baroiu ^{1,2}, Virgil Gabriel Teodor ^{1,2,*}, Viorel Păunoiu ^{1,2}, Georgiana-Alexandra Moroșanu ^{2,3}
and Ionaș-Cătălin Dumitrescu ⁴

¹ Department of Manufacturing Engineering, “Dunarea de Jos” University of Galati, 800201 Galati, Romania; nicusor.baroiu@ugal.ro (N.B.); viorel.paunoiu@ugal.ro (V.P.)

² Research Center in Manufacturing Engineering Technology (ITCM), “Dunarea de Jos” University of Galati, 800201 Galati, Romania; alexandra.costin@ugal.ro

³ Department of Thermal Systems and Automotive Engineering, “Dunarea de Jos” University of Galati, 800201 Galati, Romania

⁴ Hydraulics and Pneumatics Research Institute INOE 2000-IHP, 040558 Bucharest, Romania; dumitrescu.ihp@fluidas.ro

* Correspondence: virgil.teodor@ugal.ro; Tel.: +40-745-253-196

Abstract: In most situations, for the proper design of a gerotor pump, numerous parameters must be taken into account: the pump geometry, the properties of the materials from which the pumps are made (Young’s modulus, Poisson’s coefficient, friction coefficients, etc.), the hydraulic characteristics of the circulated fluids (fluid density, kinematic viscosity, etc.), the working performance of the pump (speed ranges, pressure, flow rate, etc.), with greater or lesser influence on volumetric efficiency, work capacity, or energy consumption. The paper presents a study regarding the inspection of the reciprocally enwrapping surfaces of the gerotor pumps using a three-dimensional measurement technique specific to reverse engineering, which involves 3D scanning of the pump components in gearing movement. The components were measured by means of a specific software (GOM Inspect) and compared, by overlap, with the CAD models made with the help of CATIA software (CATIA V5R21). At the same time, an analytical calculation algorithm was developed for the complementarity of virtual representations. Finally, the advantages of the reverse engineering technique compared to the developed theoretical algorithm and traditional CAD design are presented.

Keywords: gerotor pump; rotor; virtual pole method; reverse engineering; GOM Scan; GOM Inspect; 3D measurement; CATIA; enwrapping profiles



Citation: Baroiu, N.; Teodor, V.G.; Păunoiu, V.; Moroșanu, G.-A.; Dumitrescu, I.-C. Reverse

Engineering Used to Profile a Gerotor Pump Rotor. *Appl. Sci.* **2023**, *13*, 11069. <https://doi.org/10.3390/app131911069>

Academic Editor: Satoru Okamoto

Received: 6 September 2023

Revised: 20 September 2023

Accepted: 28 September 2023

Published: 8 October 2023



Copyright: © 2023 by the authors. Licensee MDPI, Basel, Switzerland. This article is an open access article distributed under the terms and conditions of the Creative Commons Attribution (CC BY) license (<https://creativecommons.org/licenses/by/4.0/>).

1. Introduction

The gerotor pumps with trochoidal (cycloidal, epitrochoidal, hypotrochoidal, etc.) profile rotor are special types of rotary pumps with internal gear that contain a profile, most often called a straight cycloidal profile, having a rotor consisting of two components: one known as an inner rotor and the other as an outer rotor [1–3]. The inner rotor and outer rotor come into contact with each other and create a gap between them and as the pump enters operating mode, the volume of the gap expands and shrinks continuously. The expansion of the gap creates a vacuum, and the fluid is drawn into the pump. As the gap shrinks, compression occurs, and the fluid is pumped out [4,5]. The inner rotor is fixed to the pump drive shaft and acts as the outer rotor. The inner rotor has four or more lobes (Z_1), while the outer rotor has one more lobe (Z_2) than the inner one and therefore rotates at $n/(n + 1)$ rotations per minute, orbital or satellite [6]. Although they have a lower efficiency and work at pressures of up to 150 bar, they are found in lubrication systems or as compensation pumps (booster pumps) located on the same shaft as the main pump. For these reasons, these constructions are used, in particular, as motors, being superior in many ways to classic hydrostatic motors, even if the operating principle remains similar to pumps in terms of the conversion of mechanical energy (in the form of moment and speed) into hydraulic energy (pressure and flow) [7].

F.L. Litvin [8] defined, from a geometrical point of view, the main profiles of the gearing components, with applicability to cycloidal gears. Also based on a method derived from the gearing theory, G. Bonandrini [9] analyzed the epitrochoidal and hypotrochoidal profiles, defining synthetic equations that led to the calculation of some performance indices such as the specific flow rate, the volumetric compression ratio, or the pressure angle. A. De Martin et al. [10] define and extend a study regarding the use of geometric profiles of asymmetric lobes formed by elliptical arcs, with multiple advantages over the traditional profile, while S.H. Lee et al. [11] propose a new gerotor with the shape of a lobe with 2 expanded cardioids in order to reduce the noise of the oil pump used in automatic automobile transmissions. For the efficiency of the gerotor pumps for various industrial applications, a great emphasis was placed on the geometry of gerotor pump rotors and the role they have in increasing the performance of hydraulic machines [12–15], and modeling and simulations of several gerotor pump geometries and kinematics were realized, whose results were compared with experimentally obtained values [16–20].

C.F. Hsieh [21] used finite element analysis to demonstrate theoretical calculations regarding the influence of the profile geometry of the gerotor pump lobes on stress variation and volumetric flow results.

S.M. Kwon et al. [22,23] used a computer-aided design program developed in the C++ language to define the inner profile of the rotor as a combination of two circular arcs, as well as a genetic algorithm as a technique to optimize the wear rate proportional factor. Another genetic algorithm was also used by A. Robison [24], through which he studied the pitting in a pump with the circular geometry of the gerotor gearing.

Obviously, not only the geometry of the rotor profile has a decisive role in the good operation and efficiency of such hydraulic constructions; the influence of the characteristics of the transported fluids, such as the density of the fluid or the kinematic viscosity, but also the mechanical characteristics and the physical working quantities, such as the flow rate, pressure, or working speed, they also have an extremely important role [25–28]. To ensure a smooth rotation, the profiles of the inner and outer elements of all gerotors, regardless of the number of lobes, are conjugate to each other, meaning the common normal at all contact points between the two elements passes through a fixed point, thus maintaining a constant angular speed [29]. Studying the energy efficiency problems of these pumps involves establishing mathematical models of their profiles, comparing various geometric parameters [30], or using simulations and graphical methods [31–37]. Although the construction of the pumps is robust enough, operational incidents can sometimes lead to damage to the fluid drive elements through more or less uniform wear of some of the lobes as an effect of the erosive process due to the working environment or the cavitation phenomenon as a result of the turbulent flow through the pump body of the working fluids.

In this way, in order to reconstruct such components of the pumps, it starts with the identification of the shape, usually of the solid 3D model, starting from the existing construction, identifiable by measurement, in the discrete form of the active surfaces of the rotor, using working methods specific to reverse engineering. Basically, reverse engineering is the process of analyzing an object or an environment in the real world in order to collect data on its shape, structure, and appearance so that it can be used later to build digital 3D models [38]. By means of such a technique, Zhang et al. [39] established the parametric equation of the theoretical contour curve by analyzing the radius of curvature of the cycloidal gearing using NX10.0 software. Reverse engineering problems have been developed in graphical design environments [40–42], with applications, especially in the field of virtual modeling of generating tools of pumps and compressors rotor channels or of different working components whose profiles comprise different shapes, such as circular arcs, straight segments, helical curves, involute-cycloids, cycloidal curves, or various non-analytical curves [43,44], in which profiling solutions were proposed using a set of software products, such as MATLAB for calculation and CATIA for virtual representation.

The existing problem in the reconditioning processes of rotors within pumps consists in making the tools that generate the profiles of the rotors, starting from the existing

physical characteristics, for which, often, there is no specific technical documentation. In such situations, the constructive form of the rotors can be obtained by actually measuring them, making 3D models of the rotors, and, starting from them, by profiling the generating tools with which the profiles of the parts will be processed.

The specialized literature has addressed multiple and various aspects regarding the study of gerotor pumps, a fact that makes this topic still relevant. However, from the point of view of reverse engineering techniques, there are no approaches that clearly highlight the 3D geometry of the pump components through non-contact optical methods and 3D analysis of deviations in relation to a nominal mathematical model. Thus, the technique used in this paper has an essential role in the correlation of images, respectively the projection of light fringes, intended for measuring 3D surfaces with the possibility of performing measurements in hostile environmental conditions (dust, high humidity, vibrations, large temperature variations), to which is added the speed of generating 3D surfaces of digitized objects, materialized through a network of polygons (3D mesh).

The paper highlights the advantages of the use of reverse engineering techniques versus theoretical algorithms and traditional CAD design, obtaining a reduced time for the creation of numerical models of pump rotors, the possibility of redesigning these rotors in order to improve the volumetric efficiency of the pump, and the ability of the “virtual pole” method to be applied in the study of the specific enwrapping problems of hydraulic pump profiles.

2. Materials and Methods

A study regarding the inspection of the reciprocally enwrapping surfaces of gerotor pumps is presented using a three-dimensional measurement technique specific to reverse engineering, which involves 3D scanning of the pump components in gearing movement. The components were measured by means of a specific software (GOM Inspect) and compared, by overlap, with the CAD models made with the help of CATIA software. At the same time, an analytical calculation algorithm was developed for the complementarity of virtual representations. The advantages of the reverse engineering technique compared to the theoretical algorithm and traditional CAD design are presented: reduced time in transposing the models into digital form, accurate determination of deviations by comparison with the CAD model, speed in processing the results, etc.

2.1. The Scanning Process of the Gerotor Pump Components

By using 3D scanning, a three-dimensional digital representation of the complex components of a gerotor pump is obtained, capturing in detail their shape and geometry. This information is used to evaluate the conformance of parts to specifications, to detect and analyze deviations or defects, or to perform comparisons between parts to ensure product uniformity and quality. In the present study, the ATOS Core equipment, developed by the GOM company [45], was used to establish the physical and dimensional characteristics of an inner rotor with four lobes (Z_4), while the outer rotor has an extra lobe (Z_5) compared to the inner one (Figure 1).

By using the ATOS Core equipment, the components of the gerotor pump were scanned in detail, and the 3D data obtained was used for the analysis of their geometry. Thus, the dimensions, shapes, surfaces, and other characteristics of the components were evaluated. The resulting images during scanning were processed using the GOM Scan software, which offers solutions adapted to the areas of reverse engineering and rapid prototyping, facilitating the transformation of scan data into three-dimensional digital models. The software uses advanced algorithms to faithfully reproduce the geometry of the scanned object, resulting in an accurate and detailed digital model. In order to achieve complete digitalization of the components, several scans were performed from different angles.

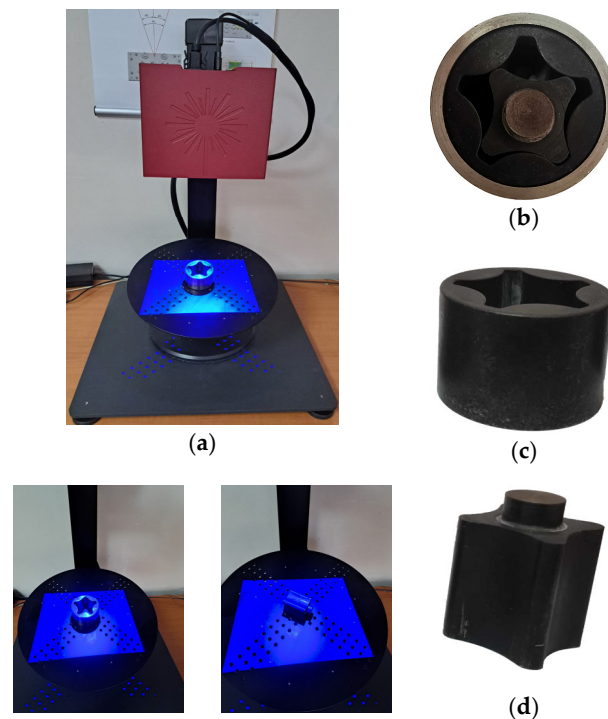


Figure 1. ATOS Core equipment (a); Gerotor pump—physical model (b); Gerotor pump components: outer rotor (c); inner rotor (d).

These scans were then integrated into a single series of measurements so as to provide a complete and detailed picture of the digitalized object. Therefore, 16 scans resulted for the inner rotor and 21 scans for the outer rotor.

After each component was completed, polygonalization was performed, a step that involved joining all scans of the two parts and obtaining complete numerical models. The resulting files were saved in *.stl format so that they could be opened and used in various software design programs such as CATIA, AutoCAD, SolidWorks, etc.

2.2. Inspection of Gerotor Pump Components

The GOM Inspect program from ATOS Core [45] allows the evaluation and analysis of data obtained by measuring with the laser scanner and the creation of precise geometric elements that allow a detailed analysis of the shape and dimensions of the measured parts. The system, defined by the measurement accuracy of the 3D coordinates of minimum $\pm 10 \mu\text{m}$ on the useful measurement volume, certified by a metrological verification bulletin of the manufacturer, the resolution of the optical sensors of minimum 5 Mpixels, respectively, the density of point clouds (inter-point distance) of maximum 0.08 mm, makes this system an excellent measuring tool where possible errors will not affect the measurement results [45]. Thus, in order to determine the dimensions of the inner and outer rotors of the gerotor pump, the contour of the two parts was built with the help of the *Single Section* command from the inspection program (Figure 2).

Thus, having identified the contours of the two parts of the gerotor pump, their dimensions can be determined in order to model them in the CATIA software program.

a. the inner rotor: To determine the outer diameter of the inner rotor, 3 points are built on the surface of the inner rotor and by means of the *3-Point Circle* command; its value can be established (Figure 3); in order to determine the shape of the active profile of the inner rotor, points are built on the contour of the part, at a distance of 2 mm between them, using the *Equidistant Points* command; at the same time, to determine the inner diameters, circles are built with the help of the *Fitting Circle* command; to determine the lengths of the part, points are built on the contour of the inner rotor with the help of the *Point* command from

the GOM Inspect program, with the distances being obtained with the help of *Distance* and *Projected Point Distance* commands.

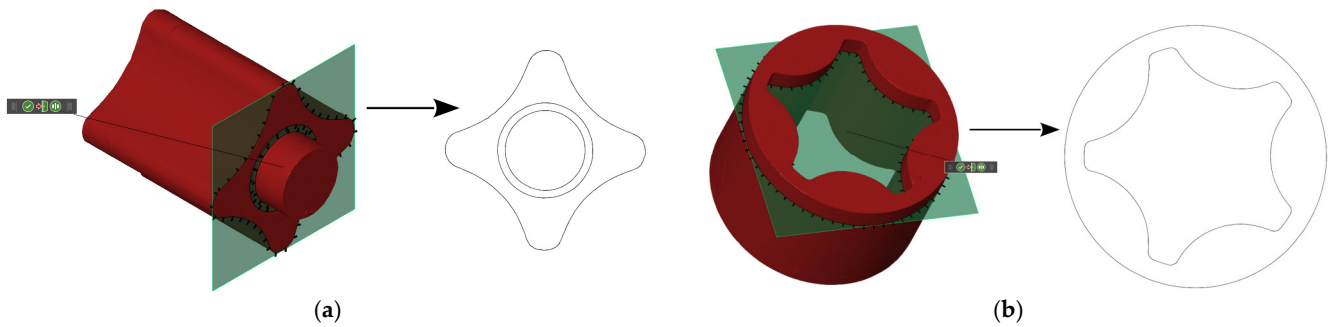


Figure 2. The construction of the contour of the inner rotor, having the Z plane as a reference plane (a); The construction of the contour of the outer rotor, having the Z plane as a reference plane (b).

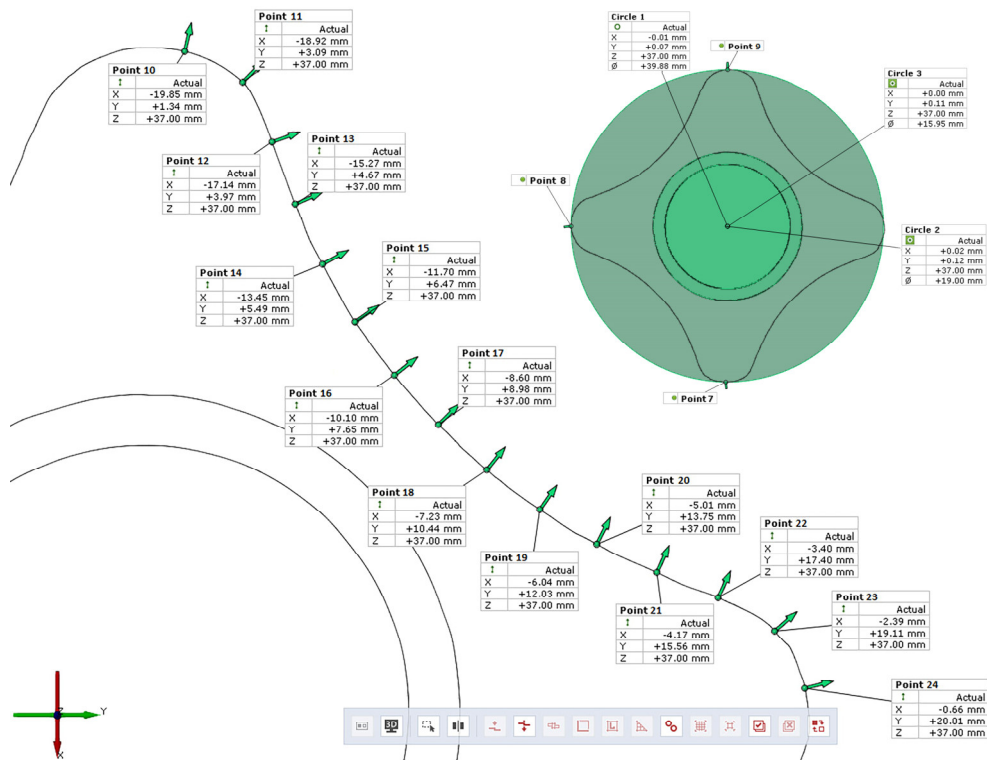


Figure 3. Determination of the shape of the active profile of the inner rotor; determining the outer diameter of the inner rotor (detail).

b. the outer rotor: To determine the outer rotor diameter, a circle is built on the contour of the part by means of the *Fitting Circle* command (Figure 4); in order to determine the shape of the active profile of the outer rotor, points are built on the contour of the part, at a distance of 2 mm between them, using the *Equidistant Points* command; to determine the length of the part, 2 points are constructed on the outer rotor surface using the *Point* command, with the distances being obtained using the *Distance* command.

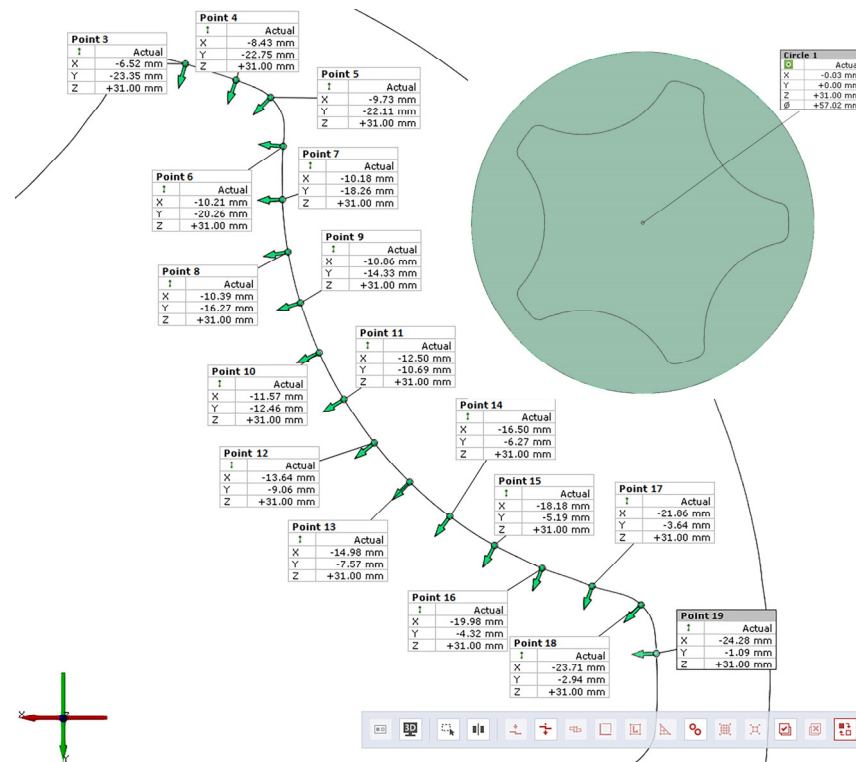


Figure 4. Determination of the shape of the active profile of the outer rotor; determining the outer rotor diameter (detail).

2.3. CAD Modeling of the Gerotor Pump

For the three-dimensional modeling of the gerotor pump elements, it is aimed to address both the CAD model itself and the profiling of the generating tools by enwrapping the ordered curls of surfaces (profiles) associated with a couple of rolling axodes (centrodes), as well as the problem of enwrapping surfaces using exclusively the facilities offered by the graphical design environment CATIA [35,41,42]. The application of the graphical method in the graphical design environment CATIA to solve a reverse engineering problem related to tools generating surfaces in reciprocal movement starts from the dimensions known by direct measurement and virtually modeled in CATIA.

The graphical model of the inner rotor and the outer rotor of the gerotor pump was generated in CATIA based on the elements measured with GOM Inspect, Figures 5 and 6, the modeling involving, for example, the generation of 77 points on the profile of the active part of the outer rotor, the coordinates of the points indicating their position in the XY reference system.

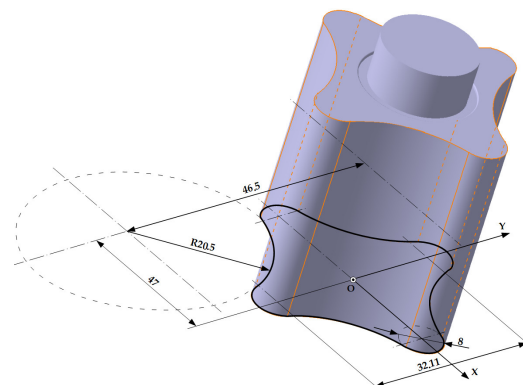


Figure 5. CATIA 3D model of the inner rotor.

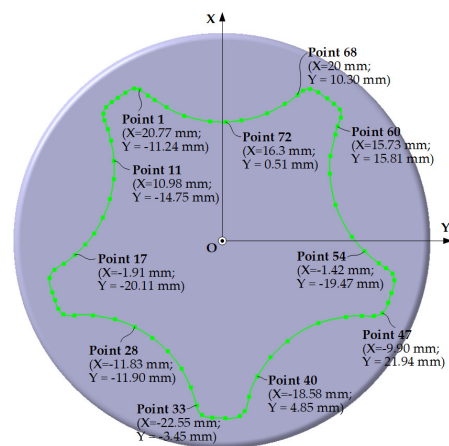


Figure 6. Points on the profile of the active part of the outer rotor.

After the modeling process is complete, the parts will be saved in *.stp format, which allows them to be opened in the GOM Inspect program. This step is essential to compare the CAD model with the scanned model of each part and assess their level of conformity and accuracy.

3. Results

3.1. CAD Model vs. Scanned Model of the Inner Rotor and the Outer Rotor

The comparison between the CAD model and the scanned model, for both the inner and outer rotor, is carried out in the GOM Inspect program. To carry out the inspection process of the inner rotor and outer rotors, it is necessary to align the actual model of the parts, obtained by scanning, with the nominal model generated by CAD modeling.

This alignment process ensures a correspondence between the two data sets and allows the evaluation of the deviations between them.

In order to carry out this procedure, the *Prealignment* command is used, since the two models (the scanned model and the CAD model), at the time of their import into the GOM Inspect program, have different orientations according to the reference system specified in the program, and it is necessary to overlap them in a single reference system (Figure 7).

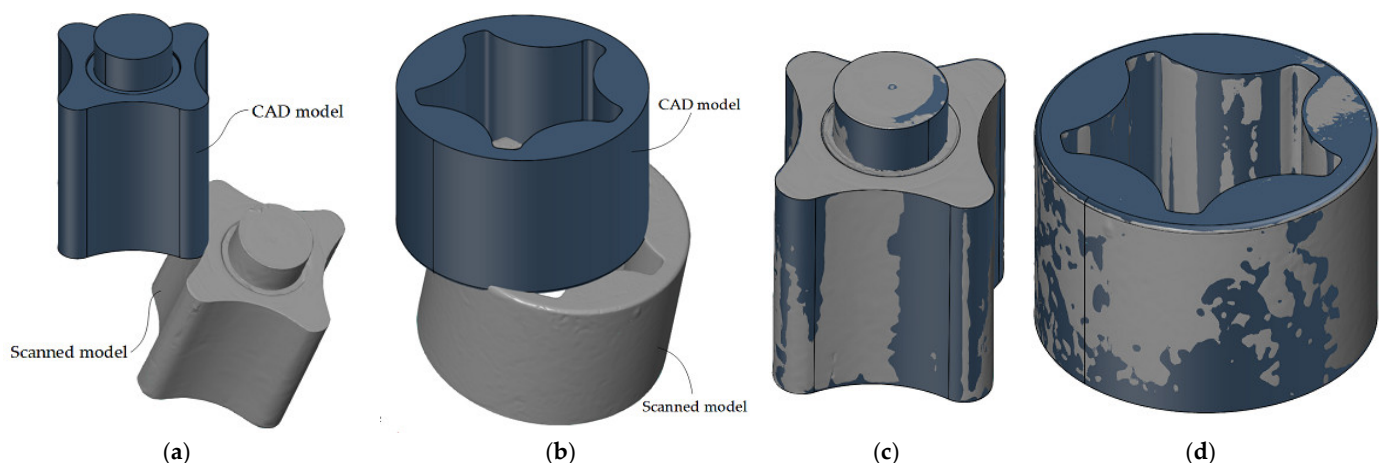


Figure 7. Orientation of the scanned model and the CAD model of the inner rotor (a) and outer rotor (b) when they are imported into the GOM Inspect program, as well as the overlap of the two models: inner rotor (c) and outer rotor (d).

After the alignment, the parts are inspected. This process involves analyzing and determining the deviations between the actual model and the nominal model. The result of

the inspection process is given in the form of a map of deviations, where each deviation is visually represented using colors.

On the deviation map, negative deviations are symbolized with a blue color, indicating a deviation below the nominal values. Zero deviations are represented in green, signifying a perfect match between the actual and nominal models. Positive deviations are highlighted in red, signifying a deviation above the nominal values (Figure 8). Areas where the deviation could not be calculated or measured are marked with a gray color.

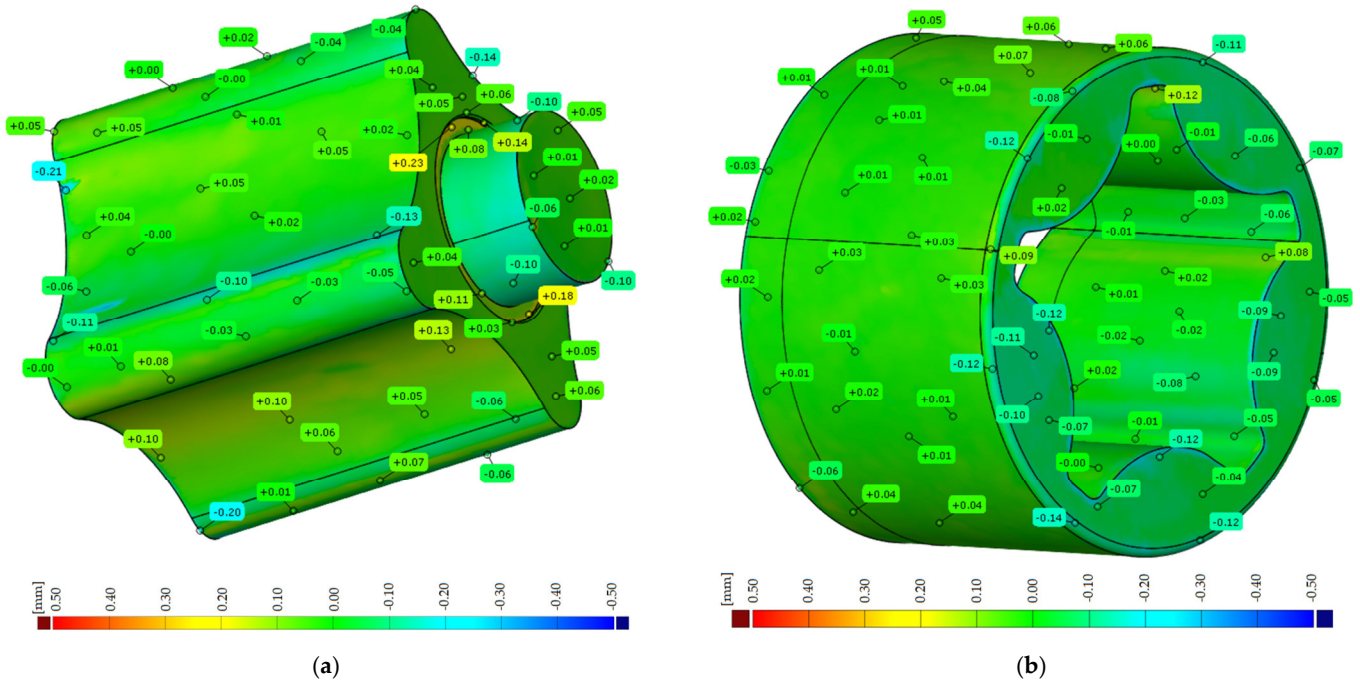


Figure 8. The map of deviations between the scanned model and the CAD model for the inner rotor (a) and the outer rotor (b).

3.2. Study of the Entwrapping Profiles of Z_4/Z_5 Gerotor Pump Rotors

The determination of the sections where the fluid accumulates during its transport from suction to discharge can be defined from the analysis of the hatched active section in Figure 9, which is delimited by two hypocycloides *I* and *II* [46].

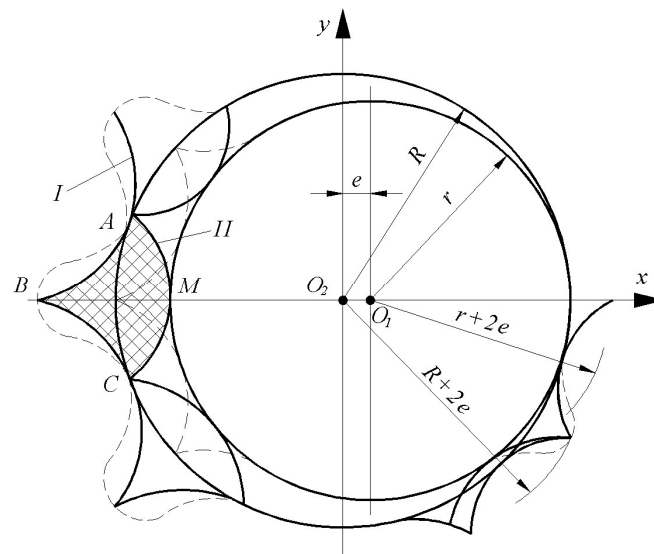


Figure 9. Active section in the gerotor pump delimited by two hypocycloides [46].

In addition to the established hypocycloidal profile models, circular arc models are also used for rotor profiles [10,15,47].

Analyzing the dimensions obtained by measurement, the following values were identified (see also Figure 5): $A_{12} = 3.8$ mm; $r = 16$ mm; $R_0 = 32.26$ mm.

These values are established in the reference systems shown in Figure 10 and whose meaning is: $x_1O_1y_1$ is the fixed reference system, having its origin in the rotation center of the Z₅ rotor, O_1 point; $x_2O_2y_2$ is the fixed reference system, having its origin in the rotation center of the Z₄ rotor, O_2 point; $X_1O_1Y_1$ is a mobile reference system, joined with the Z₅ rotor. Initially, it has the axes superimposed on the $x_1O_1y_1$ system. The $X_2O_2Y_2$ system is the mobile reference system, joined with the Z₄ rotor, and has the axes superimposed on the $x_2O_2y_2$ system at the initial moment.

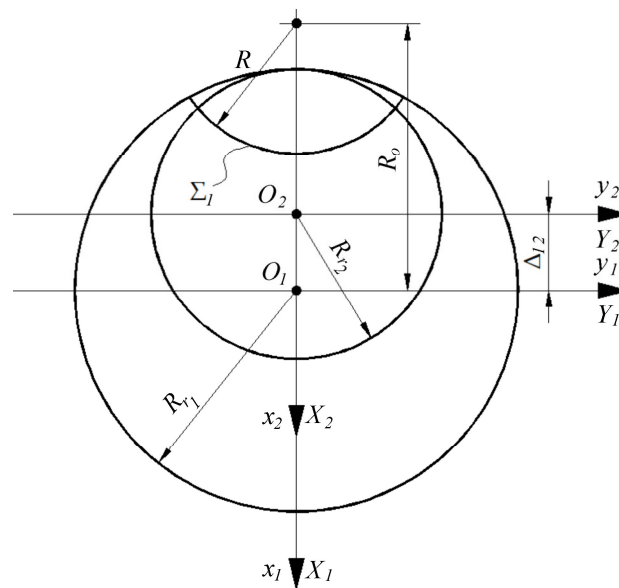


Figure 10. Reference systems for the Z₄–Z₅ rotors.

Assuming that the two profiles of the rotors are reciprocally enwrapping curves, which would ensure perfect contact between them during operation and therefore maximum efficiency of the gerotor pump, it follows that the profiles can be associated with a couple of rolling centrodes.

The two centrodes are circles, with centers at O_1 and O_2 points and radii R_{r1} and R_{r2} .

From the condition that the distance between the centers of the rolling circles is $A_{12} = R_{r1} - R_{r2}$ and from the condition that the ratio of the rolling radii is equal to the ratio of the lobe numbers of the two rotors, the values of the rolling radii can be determined:

$$\left. \begin{aligned} R_{r1} - R_{r2} &= A_{12} \\ \frac{R_{r1}}{R_{r2}} &= \frac{5}{4} \end{aligned} \right\} \Rightarrow R_{r1} = 5 \cdot A_{12}; R_{r2} = \frac{4}{5} \cdot R_{r1}. \tag{1}$$

The values are obtained: $R_{r1} = 19$ mm, $R_{r2} = 15.2$ mm.

3.3. Verification of the Minimum Rolling Radius

In order to be able to ensure enwrapping along the entire length of the two profiles, the rolling radius of each of the two centrodes should exceed the value of the minimum rolling radius. The minimum rolling radius for a certain profile is the radius of the circle that admits a tangency point with the normal to the considered profile, the normal taken through the limit point of the profile, Figure 11 [48].

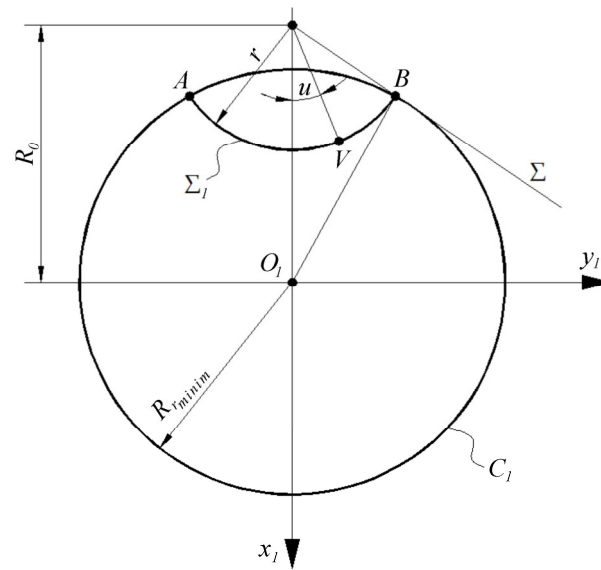


Figure 11. Defining the minimum rolling radius.

In order to determine the minimum rolling radius, it starts from the equations of the analyzed profile, Σ_1 profile:

$$\Sigma_1 \begin{cases} X_1 = -R_0 + r \cdot \cos u; \\ Y_1 = r \cdot \sin u. \end{cases} \tag{2}$$

In Equation (2), u is the angular parameter describing the Σ_1 profile.

The tangent to the Σ_1 profile has the equation:

$$t - t \left| \frac{X - X(u)}{\dot{X}_u} = \frac{Y - Y(u)}{\dot{Y}_u} \right.; \tag{3}$$

$$\dot{X}_u = -r \cdot \sin u; \dot{Y}_u = r \cdot \cos u. \tag{4}$$

Taking into account the profile Equation (2), Equation (3) becomes:

$$\frac{X + R_0 - r \cdot \cos u}{-r \cdot \sin u} = \frac{Y - r \cdot \sin u}{-r \cdot \cos u} \tag{5}$$

or, developed:

$$Y = \frac{r - R_0 \cdot \cos u - X \cdot \cos u}{\sin u}. \tag{6}$$

The normal to the Σ_1 profile, which passes through the O_1 origin, has the equation:

$$n - n : X \cdot \dot{X}_u + Y \cdot \dot{Y}_u = 0; \tag{7}$$

$$-X \cdot r \cdot \sin u + Y \cdot r \cdot \cos u = 0; \tag{8}$$

$$-X \cdot \sin u + \frac{r \cdot \cos u}{\sin u} - \frac{R_0 \cdot \cos^2 u}{\sin u} - \frac{X \cdot \cos^2 u}{\sin u} = 0; \tag{9}$$

$$\frac{-X}{\sin u} = \frac{R_0 \cdot \cos^2 u - r \cdot \cos u}{\sin u}; \tag{10}$$

$$\begin{aligned} X &= r \cdot \cos u - R_0 \cdot \cos^2 u = (r - R_0 \cdot \cos u) \cdot \cos u; \\ Y &= \frac{r - R_0 \cdot \cos u - (r - R_0 \cdot \cos u) \cdot \cos u}{\sin u} = (r - R_0 \cdot \cos u) \cdot \sin u. \end{aligned} \tag{11}$$

The minimum rolling radius is mathematically defined as the maximum distance between the current point on the Σ_1 profile and the intersection point between the tangent to Σ_1 at the current point and the normal to Σ_1 , which passes through the origin of the reference system (O_1). If this distance is noted by Δ , this is obtained:

$$\begin{aligned} \Delta &= \left[(-R_0 + r \cdot \cos u - r \cdot \cos u + R_0 \cdot \cos^2 u)^2 + (r \cdot \sin u - r \cdot \sin u + R_0 \cdot \sin u \cdot \cos u)^2 \right]^{1/2}, \\ \Delta &= \left(R_0^2 \cdot \sin^4 u + R_0^2 \cdot \sin^2 u \cdot \cos^2 u \right)^{1/2}, \\ \Delta &= R_0 \cdot \sin u. \end{aligned} \tag{12}$$

The value of the minimum rolling radius will be:

$$R_{r\min} = R_0 \cdot \sin u_{\max}. \tag{13}$$

For the previously calculated rolling radius value R_{r1} ($R_{r1} = 19$ mm), it means that the last point on the Σ_1 profile in which it is in a reciprocally enwrapping relation with the Σ_2 profile corresponds to the angle $u_{\max} = 36.42^\circ$.

The profile area (S) between the points A —corresponding to $u = 36.42^\circ$ and B —corresponding to $u = 42.1^\circ$ will not be in contact during rolling with the Σ_2 profile; therefore, there will be a volume of uncirculated fluid.

For the dimensions measured, this fluid volume is approximately 200 mm³ (Figure 12).

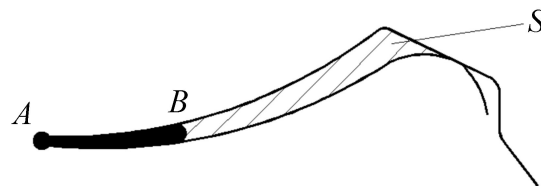


Figure 12. Defining the active surface area (S) occupied by the fluid.

3.4. Modifications in Order to Increase the Efficiency of the Pump

In order to increase the efficiency of the pump, a series of modifications are proposed to reduce the volume of recirculated fluid. These changes were made taking into account the current construction of the pump, following a minimum of changes for the component elements.

A first modification involves increasing the rolling radius until reaching the minimum rolling radius value at the extreme point of the Σ_1 profile, a point that corresponds to the angle $u = 42.1^\circ$.

Therefore, the rolling radius must be $R_{r1} = R_0 \cdot \sin u = 32.26 \cdot \sin u = 21.47$ mm.

This also implies changing the R_{r2} and A_{12} values: $R_{r2} = 4/5 \cdot R_{r1} = 17.176$ mm; $A_{12} = R_{r1} - R_{r2} = 4.4$ mm. $R_{r1} = 22$ mm and $R_{r2} = 17.6$ mm are adopted.

Changing the distance between the centers of the rolling circles can be carried out by inserting an eccentric bushing or rebuilding the pump stator. Changing the Σ_2 profile implies a total change in the Z_4 rotor.

3.5. Optimized Profile of the Z_4 Rotor

For the calculation of an optimized profile of the Z_4 rotor, the reciprocally enwrapping profile to the existing Σ_1 profile is calculated. The radii of the two centroids associated with the rolling profiles Σ_1 and Σ_2' will be $R_{r1} = 22$ mm and $R_{r2} = 17.6$ mm.

$$\Sigma_1 \left| \begin{aligned} X &= -R_0 + r \cdot \cos u; \\ Y &= r \cdot \sin u. \end{aligned} \right. \tag{14}$$

The normal to Σ_1 has the equation:

$$\bar{N}_\Sigma = \lambda (\dot{Y}_u \cdot \bar{i} - \dot{X}_u \cdot \bar{j}), \tag{15}$$

with $\dot{X}_u = -r \cdot \sin u$; $\dot{Y}_u = r \cdot \cos u$ (4). In these conditions:

$$\bar{N}_\Sigma = \lambda \cdot r \cdot \cos u \cdot \bar{i} + \lambda \cdot r \cdot \sin u \cdot \bar{j}. \tag{16}$$

The position vector of the current point on Σ_1 is

$$\bar{r} : X(u) \cdot \bar{i} + Y(u) \cdot \bar{j} = (-R_0 + r \cdot \cos u) \cdot \bar{i} + r \cdot \sin u \cdot \bar{j}. \tag{17}$$

The “virtual pole” method is used to determine the reciprocally enwrapping profile. The “virtual pole” basically represents an intersection point between the normal to a profile that belongs to the generated blank and a centrode associated with the blank (part), the centrode representing the geometric locus of the instantaneous centers in the movement of a plane figure [49,50]:

$$\begin{aligned} \bar{r}_{P_V} &= \bar{N}_\Sigma + \bar{r} = (-R_0 + r \cdot \cos u) \cdot \bar{i} + r \cdot \sin u \cdot \bar{j} + \lambda \cdot r \cdot \cos u \cdot \bar{i} + \lambda \cdot r \cdot \sin u \cdot \bar{j} = \\ &= (-R_0 + r \cdot \cos u + \lambda \cdot r \cdot \cos u) \cdot \bar{i} + (r \cdot \sin u + \lambda \cdot r \cdot \sin u) \cdot \bar{j} \end{aligned} \tag{18}$$

The C_1 centrode has the equations:

$$C_1 : \begin{cases} X = -R_{r_1} \cdot \cos \varphi_1; \\ Y = R_{r_p} \cdot \sin \varphi_1. \end{cases} \tag{19}$$

The scalar λ is removed from the equations, and the relation between the parameters u and φ_1 is determined.

$$\begin{cases} -R_{r_1} \cdot \cos \varphi_1 = -R_0 + r \cdot \cos u + \lambda \cdot r \cdot \cos u; \\ R_{r_1} \cdot \sin \varphi_1 = r \cdot \sin u + \lambda \cdot r \cdot \sin u; \end{cases} \tag{20}$$

$$\lambda = \frac{-R_{r_1} \cdot \cos \varphi_1 \cdot \sin \varphi_1 + R_0}{r \cdot \cos u} = \frac{R_{r_1} \cdot \sin \varphi_1 - r \cdot \sin u}{r \cdot \sin u}; \tag{21}$$

$$\begin{aligned} -R_{r_1} \cdot \cos \varphi_1 \cdot \sin u + R_0 \cdot \sin u - r \cdot \cos u \cdot \sin u &= \\ = R_{r_1} \cdot \sin \varphi_1 \cdot \cos u - r \cdot \sin u \cdot \cos u; \end{aligned} \tag{22}$$

$$-R_{r_1} \cdot (\cos \varphi_1 \cdot \sin \varphi_1 + \sin \varphi_1) = R_0 \cdot \sin u; \tag{23}$$

$$\varphi_1 = \left[\arcsin \left(\frac{R_0 \cdot \sin u}{R_{r_1}} \right) \right] - u; \tag{24}$$

$$u = \arcsin \left(\frac{Y_i}{r} \right) = \arctg \left(\frac{Y_i}{-R_0 + X_i} \right). \tag{25}$$

3.6. Calculation of the Enwrapping Profile

In order to determine the coordinates of the C_1 point on the Z_4 rotor, which is in enwrapping with the C_2 point on the Z_5 rotor, the “virtual pole” method is used.

Using the enwrapping condition, the value of the φ_1 angle for which the normal to the Σ_1 profile, taken through the C_1 point, passes through the gearing pole is established. For $u = 42.1^\circ$, it results $\varphi_1 = \left[\arcsin \left(\frac{32.26 \cdot \sin 42.1^\circ}{22} \right) \right] - 42.1^\circ$, so $\varphi_1 = 37.348^\circ$.

When the $X_1O_1Y_1$ system rotates by the φ_1 angle, the normal passes through the gearing pole, and the coordinates of the C_1 point in the $x_1O_1y_1$ system will be given by the coordinate transformation:

$$x_1 = \omega_3^T(\varphi_1) \cdot X_1; \tag{26}$$

$$\begin{pmatrix} x_1 \\ y_1 \end{pmatrix} = \begin{pmatrix} \cos \varphi_1 & -\sin \varphi_1 \\ \sin \varphi_1 & \cos \varphi_1 \end{pmatrix} \cdot \begin{pmatrix} X_1 \\ Y_1 \end{pmatrix} = \begin{pmatrix} X_1 \cdot \cos \varphi_1 - Y_1 \cdot \sin \varphi_1 \\ X_1 \cdot \sin \varphi_1 + Y_1 \cdot \cos \varphi_1 \end{pmatrix}. \tag{27}$$

For $u = 42.1^\circ$, it results in

$$\begin{cases} X_1 = -R_0 + r \cdot \cos u = -20.388; \\ Y_1 = r \cdot \sin u = 10.72; \end{cases}$$

$$\begin{cases} x_1 = X_1 \cdot \cos \varphi_1 - Y_1 \cdot \sin \varphi_1 = -30.294; \\ y_1 = X_1 \cdot \sin \varphi_1 + Y_1 \cdot \cos \varphi_1 = -3.846. \end{cases}$$

In the $x_2O_2y_2$ system, the coordinate point x_1y_1 , previously calculated, has the coordinates:

$$x_2 = x_1 + A; \tag{28}$$

$$\begin{pmatrix} x_2 \\ y_2 \end{pmatrix} = \begin{pmatrix} x_1 \\ y_1 \end{pmatrix} + \begin{pmatrix} A_{12} \\ 0 \end{pmatrix}. \tag{29}$$

For $u = 42.1^\circ$, it results in $\begin{pmatrix} x_2 \\ y_2 \end{pmatrix} = \begin{pmatrix} -30.294 + 4.4 \\ -3.846 \end{pmatrix} = \begin{pmatrix} -25.894 \\ -3.846 \end{pmatrix}$.

This point corresponds to a φ_2 rotation of the $X_2O_2Y_2$ system, with the value of φ_2 being given by

$$R_{r_1} \cdot \varphi_1 = R_{r_2} \cdot \varphi_2. \tag{30}$$

It results in $\varphi_2 = \frac{R_{r_1}}{R_{r_2}} \cdot \varphi_1 = \frac{5}{4} \cdot \varphi_1 = 46.685^\circ$. Therefore, the coordinates of this point in the $X_2O_2Y_2$ system will be

$$X_2 = \omega_3(\varphi_2) \cdot x_2; \tag{31}$$

$$\begin{pmatrix} X_2 \\ Y_2 \end{pmatrix} = \begin{pmatrix} \cos \varphi_2 & \sin \varphi_2 \\ -\sin \varphi_2 & \cos \varphi_2 \end{pmatrix} \cdot \begin{pmatrix} x_2 \\ y_2 \end{pmatrix} = \begin{pmatrix} x_2 \cdot \cos \varphi_2 + y_2 \cdot \sin \varphi_2 \\ -x_2 \cdot \sin \varphi_2 + y_2 \cdot \cos \varphi_2 \end{pmatrix}. \tag{32}$$

In these conditions, $\begin{pmatrix} X_2 \\ Y_2 \end{pmatrix} = \begin{pmatrix} -20.562 \\ 16.202 \end{pmatrix}$.

For $u = 42.1^\circ$ and $A_{12} = 4.4$, results:

$$i = \frac{5}{4}; R_{r_1} - R_{r_2} = A_{12} = R_{r_1} - \frac{R_{r_1}}{i}; R_{r_1} = A_{12} \cdot \left(\frac{i}{i-1} \right); R_{r_2} = R_{r_1} - A_{12}.$$

It is known that $x_1 = \omega_3^T(\varphi_1) \cdot X_1$ și $\varphi_1 = \left[\arcsin\left(\frac{R_0 \cdot \sin u}{R_{r_1}}\right) \right] - u$, see relations (25) and (26), and $\varphi_2 = i \cdot \varphi_1$.

If $x_2 = x_1 + A; x_2 = \omega_3^T(\varphi_1) \cdot X_1 + A_{12}$, then

$$\begin{pmatrix} X_2 \\ Y_2 \end{pmatrix} = \begin{pmatrix} \cos \varphi_2 & \sin \varphi_2 \\ -\sin \varphi_2 & \cos \varphi_2 \end{pmatrix} \cdot \begin{pmatrix} X_1 \cdot \cos \varphi_1 - Y_1 \cdot \sin \varphi_1 + A_{12} \\ X_1 \cdot \sin \varphi_1 + Y_1 \cdot \cos \varphi_1 \end{pmatrix}. \tag{33}$$

By developing,

$$\begin{aligned}
 \begin{pmatrix} X_2 \\ Y_2 \end{pmatrix} &= \begin{pmatrix} X_1 \cdot \cos \varphi_1 \cdot \cos \varphi_2 - Y_1 \cdot \sin \varphi_2 \cdot \cos \varphi_2 + \\ -X_1 \cdot \cos \varphi_1 \cdot \sin \varphi_2 + Y_1 \cdot \sin \varphi_1 \cdot \sin \varphi_2 - \\ +A_{12} \cdot \cos \varphi_2 + X_1 \cdot \sin \varphi_1 \cdot \sin \varphi_2 + Y_1 \cdot \cos \varphi_1 \cdot \sin \varphi_2 \\ -A_{12} \cdot \sin \varphi_2 + X_1 \cdot \sin \varphi_1 \cdot \cos \varphi_2 + Y_1 \cdot \cos \varphi_1 \cdot \cos \varphi_2 \end{pmatrix} = \\
 &= \begin{pmatrix} X_1 \cdot (\cos \varphi_1 \cdot \cos \varphi_2 + \sin \varphi_1 \cdot \sin \varphi_2) - \\ X_1 (\sin \varphi_1 \cdot \cos \varphi_2 - \cos \varphi_1 \cdot \sin \varphi_2) + \\ -Y_1 (\sin \varphi_1 \cdot \cos \varphi_2 - \cos \varphi_1 \cdot \sin \varphi_2) + A_{12} \cdot \cos \varphi_2 \\ +Y_1 (\cos \varphi_1 \cdot \cos \varphi_2 + \sin \varphi_1 \cdot \sin \varphi_2) - A_{12} \cdot \sin \varphi_2 \end{pmatrix} = \\
 &= \begin{pmatrix} X_1 \cdot \cos(\varphi_1 - \varphi_2) - Y_1 \cdot \sin(\varphi_1 - \varphi_2) + A_{12} \cdot \cos \varphi_2 \\ X_1 \cdot \sin(\varphi_1 - \varphi_2) + Y_1 \cdot \cos(\varphi_1 - \varphi_2) - A_{12} \cdot \sin \varphi_2 \end{pmatrix}.
 \end{aligned}
 \tag{34}$$

Using the "virtual pole" method, the profile of the Z₄ rotor was recalculated so that it was reciprocally enwrapping around the circle arc profile of the Z₅ rotor.

The coordinates of the points on the profile of this rotor are presented in Table 1, and the trajectories passed by these points in the relative movement described by the Z₄ rotor compared to the reference system of the Z₅ rotor are highlighted in Figure 13.

Table 1. Coordinates of the redesigned Z₄ rotor profile points.

X [mm]	Y [mm]
-16.26	0
-16.2964	1.122976
-16.4052	2.241001
-16.5857	3.34923
-16.8364	4.443046
-17.1556	5.518244
-17.5408	6.571349
-17.9893	7.600286
-18.4988	8.606171
-19.0703	9.599994
-19.7401	10.66095

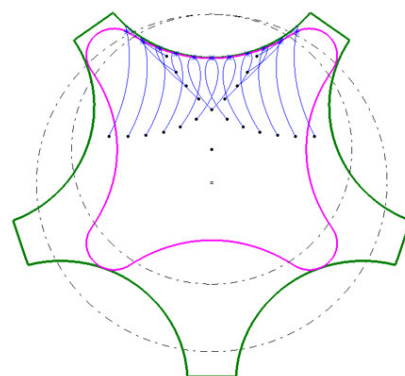


Figure 13. Trajectories of the points on the rotor profile Z₄ in relative movement to Z₅.

Figures 14 and 15 show the surfaces between the two rotors, which will lead to the existence of different volumes of pumped fluid, depending on the angular positioning of φ_2 at 0°, 30°, 60°, 90°, 120°, 150°, and 180°.

The values that define the sections of the chambers (S), in [mm²], and the distances between the outer and inner rotor profiles, right and left, in [mm], both for the initial version and for the redesigned one, are specified in Table 2, respectively, in Figures 16–18.

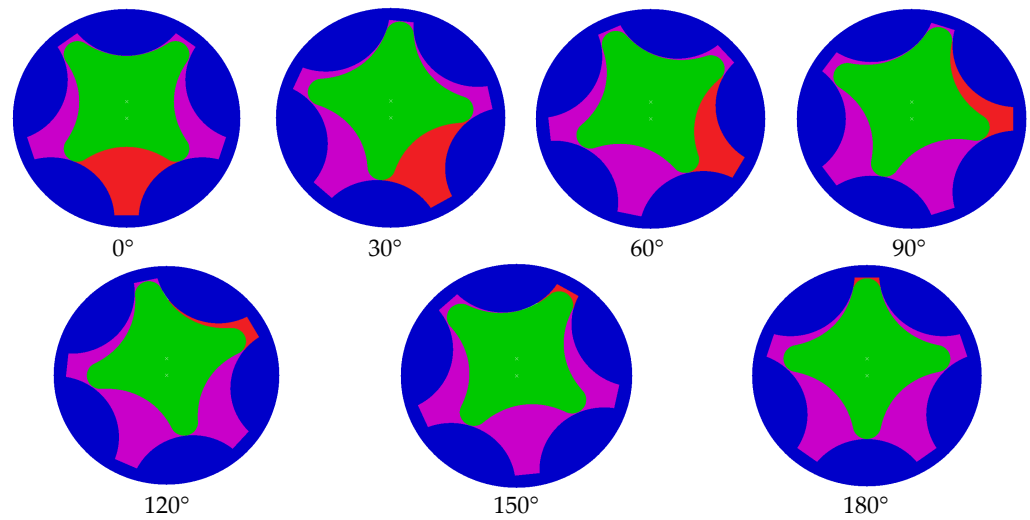


Figure 14. Defining the surfaces occupied by the fluid in rolling movement (red color)—initial version.

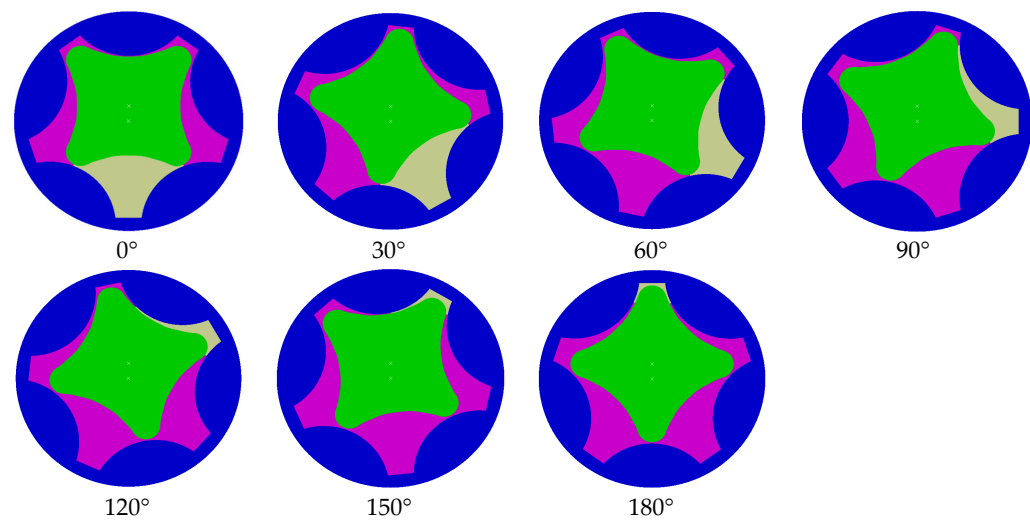


Figure 15. Defining the surfaces occupied by the fluid in rolling movement (grey color)—redesigned version.

Table 2. The values of the sections occupied by the fluid and the distances between the profiles—initial and redesigned.

φ_2 [°]	Initial S [mm ²]	Initial d —Left [mm]	Initial d —Right [mm]	Redesigned S [mm ²]	Redesigned d —Left [mm]	Redesigned d —Right [mm]
0°	199.983	0.366	0.363	224.089	0.106	0.106
30°	183.651	0.289	0.437	204.739	0.012	0.238
60°	140.856	0.328	0.449	153.756	0.047	0.233
90°	87.181	0.461	0.392	89.807	0.182	0.108
120°	41.141	0.484	0.259	36.575	0.259	0.061
150°	16.8	0.412	0.143	10.382	0.181	0.06
180°	10.533	0.383	0.39	4.282	0.073	0.07

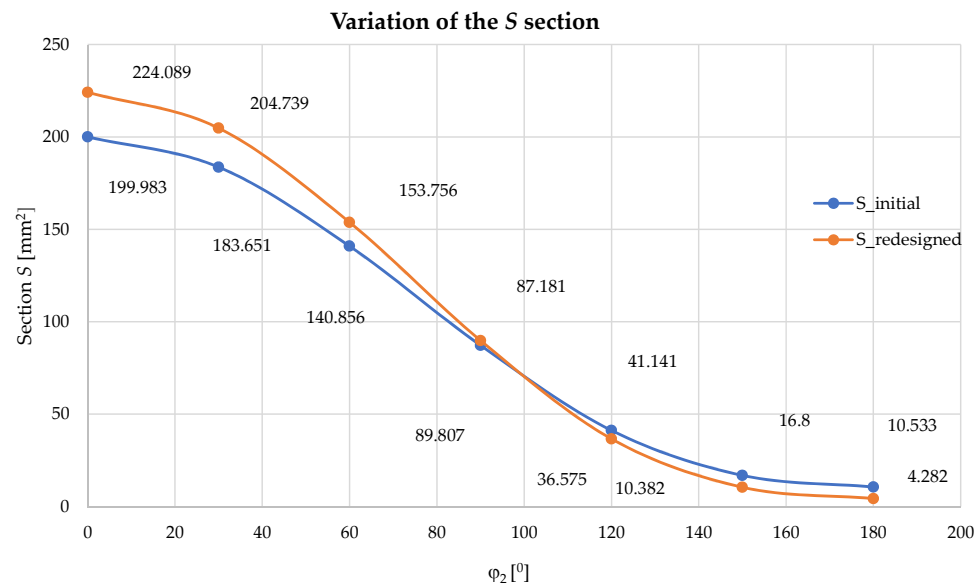


Figure 16. The variation of the values of the S occupied by the fluid depending on the angular positioning ϕ_2 .

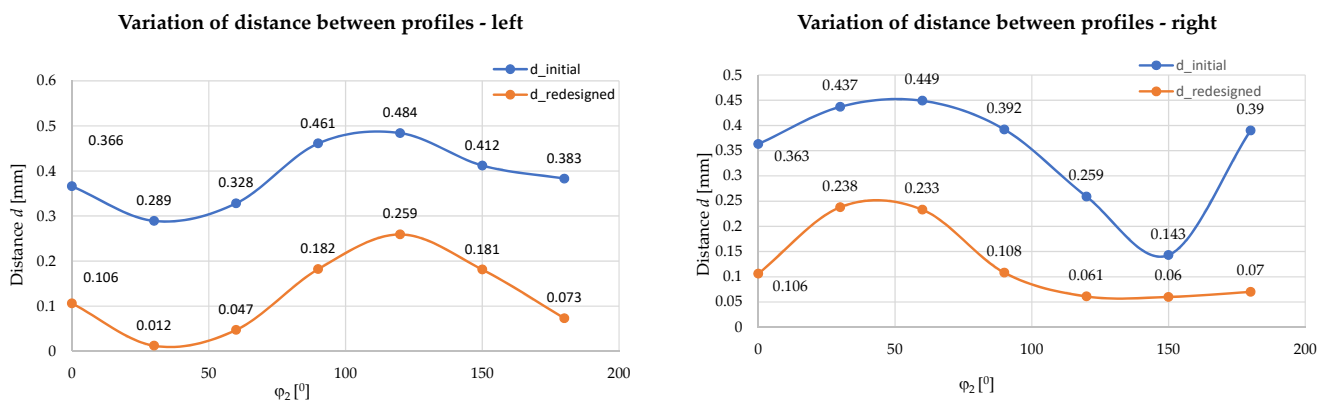


Figure 17. The variation of the values of the distances between the profiles depending on the angular positioning ϕ_2 .

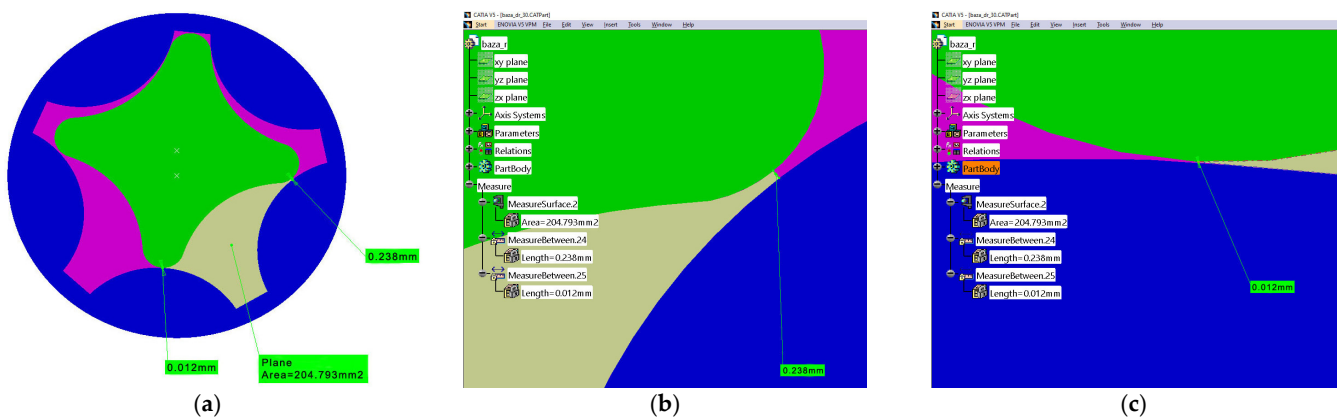


Figure 18. Distances d between the outer and inner rotor profiles: right and left (a); right (b); left (c).

In order to achieve the sealing between the two rotors, it is necessary that the radius of connection between the lobes of the Z_4 rotor be modified and, simultaneously, the

connection area between the lobes of the Z_5 rotor be modified. These changes are shown in Figure 17.

4. Discussion

The gerotor pump with internal gearing with lobes is driven by means of a control shaft where the outer Z_5 rotor is unbalanced from the Z_4 rotor and the control shaft. When the inner rotor rotates, the outer rotor is driven to rotate in the same direction. The aspirated oil into the space between the rotors is transported by the inner and outer rotor lobes in the space that shrinks due to the eccentricity and is pumped under pressure towards the fluid line.

The aim of the study was to use some original concepts regarding the possibility of improving the geometry of the rotors, starting from the known profile of one of them:

- The use of a three-dimensional measurement technique specific to reverse engineering, 3D scanning, as a developing technology, is increasingly used in dimensional quality control due to its capabilities to provide precise geometrical information for complex or assembled parts. The inspection of the reciprocally enwrapping surfaces for the rotors of the gerotor pump had the role of quickly creating a 3D model consisting of a "cloud of points" obtained after scanning the surfaces of the parts, the "cloud of points" being later used in their reconstruction (Figures 1–4). The major advantage of using the automated scanning and analysis system was that a quick and accurate inspection of the rotors could be achieved, significantly reducing the time and effort required compared to traditional manual measurement methods. At the same time, the CAD model was created based on the dimensions from the gerotor pump data sheet, respectively, based on the scanned model (Figures 5 and 6). The comparison of the two models was made by choosing the upper limit value of the represented deviations to be 0.5 mm and the lower limit value to be -0.5 mm (Figure 7), demonstrating the accuracy of the models and showing that the significant deviations that appear in Figure 8 are limited and represent exceptions. These areas of deviation are due to the imperfections present in the scanned parts and the measurement difficulties caused by their complex shape. It is important to emphasize that these deviations do not indicate errors in the numerical models obtained by design. Of course, the possibility of making a rapid comparison between the initial model and the redesigned one allows a theoretical analysis of the change in the volume efficiency of the pumps and, therefore, the increase in productivity in industrial processes.
- The use of a new complementary method of analytical profiling of enwrapping generating cutting tools, an original method called the "virtual pole" method, by which calculation errors due to writing complicated calculation equations can be avoided if the fundamental theorems and consecrated methodologies are used in order to solve the problem of profiling the generating tools. Under these conditions, the prospects are open for the application of the "virtual pole" method for the corrective profiling of tools that generate by enwrapping and also the extension of the study methods for enwrapping other types of surfaces, such as helical surfaces, by analyzing the frontal profiles of various types of hydraulic pumps.
- The use of an analytical calculation method, in this case the "virtual pole" method, has demonstrated that it can allow the second enwrapping component to be accurately redesigned when the dimensions of the other are known, provided based on the three-dimensional measurement technique specific to reverse engineering. Thus, the method was beneficial in recalculating the profile of the Z_4 rotor so that it is reciprocally enwrapped to the circle arc profile of the Z_5 rotor, as evidenced by the coordinates that define the trajectories of the points on the profile of the Z_4 rotor in relative movement to Z_5 , Figures 9–13.

The essence of the study was limited to defining two entities as comparison parameters: the surfaces where the fluid accumulates (generically defined as S), in the version of the model obtained directly by reverse engineering, respectively of the one redesigned by the

“virtual pole” method, depending on the angular positioning of the movement parameter of the mobile reference system, joined with the tool profile, respectively at 0° , 30° , 60° , 90° , 120° , 150° and 180° , Figures 14–16, respectively the distance between the inner and outer rotor profiles (generically defined as d), in the version of the model obtained directly through reverse engineering, respectively of the one redesigned using the “virtual pole” method, Figures 17 and 18.

A block diagram of the research methodology is briefly presented in Figure 19.

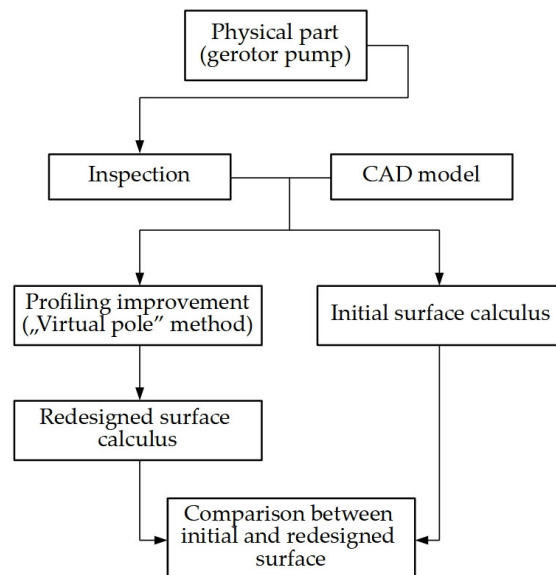


Figure 19. The block diagram of the research methodology.

The modification of the rolling radius was discussed so that the wrapping between the two active profiles (inner rotor and outer rotor) is carried out along the entire length of the profiles. It was observed that this modification also leads to an increase in the maximum surface of the space between the teeth— S (including maximum volume) h —at 0° , in which case the pump is in the suction phase and the fluid is being pumped to the next position, 30° . At the same time, at 180° , the surface S is minimal (including the volume), and the pump is in the discharge phase.

- If the rolling radius had a value lower than the value of the minimum rolling radius, then there would have been an area on the profile of the inner rotor that was not wrapped with the profile of the outer rotor.

This leads to the existence of a larger surface in position 180° , which means that there is a volume of recirculated fluid that cannot be completely removed during discharge.

- A running radius greater than the calculated minimum value would have had the effect of increasing the size of the outer and inner rotors. Due to the ease of processing, the specific recalculated values for the rolling radii of the form were adopted: $R_{r1} = 22$ mm; $R_{r2} = 17.6$ mm for $u = 42.1^\circ$.

The modification of the rolling radius values directly implies the modification of the distance between the rolling centers, A_{12} (eccentricity), resulting in a value of 4.4 mm. Conversely, any change in the distance between the centers of the rolling circles leads to a change in the rolling radii and implicitly in the surface and volume covered by the fluid, a fact that is closely correlated with the change in the geometric shapes and dimensions of both the inner and outer rotors.

From the analysis of the data obtained, it can be seen that the redesigned model decreases the distance between the rotor profiles while decreasing the final area bounded by the profiles of the Z_4 and Z_5 elements by approximately 16%, which may also imply an increase in the volume of fluid.

5. Conclusions

Multirotor pumps with gerotor technology, apart from the advantages of increasing the flow rate and balancing the radial forces, represent a balanced compromise in terms of simplicity, robustness, compactness, versatility, and noise due to the simpler structure and reduced number of components compared to other external or internal transmission pumps, which play an essential role in increasing volume yield.

The use of technologies based on advanced optical sensors and sophisticated algorithms to perform high-resolution and accurate scans can lead to the rapid and accurate acquisition of three-dimensional data, the filtering of this data, as well as its export in various formats usable in design and analysis applications, contributing to obtaining accurate and complete results in the digitalization process.

Another important aspect of using reverse engineering 3D measurement techniques is the creation of custom reports that include tables of measurement results, images of inspected parts, and relevant diagrams. These reports provide essential information about part quality and compliance and can be used in quality control, product development, and manufacturing processes.

Thus, the paper demonstrates that the use of reverse engineering techniques not only substantially reduces the time to translate physical objects into formats that can be easily edited by other software but can also generate numerical models with remarkable accuracy compared to CAD models.

- The use of three-dimensional scanning allows complex numerical models to be obtained on which geometric measurements and features can be determined, allowing an accurate and complete CAD model to be produced. By comparison, obtaining the numerical model using a coordinate measuring machine would require a higher workload and a more skilled operator. In this case, it was estimated that the time savings achieved using the ATOS measuring system compared to using a coordinate measuring machine were about 50%, since both features have relatively simple geometry. The advantage of scanning techniques increases even more with increasing part complexity and is recommended for one-off or small-series products.
- By overlapping the scanned models over the CAD models, it was observed that the upper limit value of the represented deviations is 0.5 mm and the lower limit value is -0.5 mm, demonstrating the accuracy of the models.
- The use of the “virtual pole” method, the original method, the foundations of which were laid by members of the authors’ team, facilitated the redesign of the existing models, leading to a substantial improvement by decreasing the distances d between the inner and outer rotors, which are in the enclosure, leading to better tightness between the moving components, as well as by increasing the theoretical area S in which fluid accumulates in various angular positions in the rotational motion. Thus, for the distances d a difference between 4.2% (at an angle $\varphi_2 = 30^\circ$) and 57.8% (at an angle $\varphi_2 = 120^\circ$) is observed on the left side, and 17.9% (at an angle $\varphi_2 = 180^\circ$) and 54.4% (at an angle $\varphi_2 = 30^\circ$) on the right side. In the case of the S area, overall, there is an increase of about 16% for the redesigned, improved model.

The present study opens perspectives in the design of profiling algorithms based on which high-level programming language applications can be realized, for example, Visual Basic for Applications realized in the CATIA software program, which allow the profiling of various cutting tools to contribute to the optimization of the design and manufacture of parts from the structure of volumetric pumps and not only.

Likewise, the virtual pole method has been successfully applied to the profiling of other types of cutting tools (rotary cutter designed to process ball screws, gear-shaped cutter for generating profiled holes, rack tool for generating a piece of type shaft with a square section, etc.), which can profile both components from various industrial and general environments, but also those specific to the hydro-pneumatic field (helical surfaces of hydraulic pumps, conical screws from the structure of compressors, etc.).

Author Contributions: Conceptualization, V.G.T. and N.B.; methodology, V.G.T. and N.B.; validation, N.B., V.G.T., V.P. and I.-C.D.; formal analysis, V.G.T., V.P. and N.B.; investigation, G.-A.M.; resources, V.G.T., I.-C.D. and N.B.; writing—original draft preparation, N.B., V.G.T. and G.-A.M.; writing—review and editing, G.-A.M.; visualization, N.B., V.P. and V.G.T.; supervision, N.B. and V.G.T.; project administration, V.G.T. and N.B.; funding acquisition, N.B. and I.-C.D. All authors have read and agreed to the published version of the manuscript.

Funding: This paper has also received financing under a project funded by the Ministry of Research, Innovation and Digitalization through Programme 1—Development of the national research and development system, Sub-programme 1.2—Institutional performance—Projects financing the R&D&I excellence, Financial Agreement no. 18PFE/30.12.2021 and “Dunarea de Jos” University of Galati, Romania.

Institutional Review Board Statement: Not applicable.

Informed Consent Statement: Not applicable.

Data Availability Statement: Not applicable.

Conflicts of Interest: The authors declare no conflict of interest.

Abbreviations

xy	fixed reference system
I, II	hypocycloids
e	eccentricity
BAM, BCM	partial sections
$BAMC$	total section
A_{12}	the distance between the centers of the rolling circles R_{r_1} and R_{r_2}
R_{r_1}	the rolling radius of the C_1 centrode associated with the Z_5 rotor
R_{r_2}	the rolling radius of the C_2 centrode associated with the Z_4 rotor
r	the radius of the profile of outer rotor
R_0	the distance between the rolling radius R_{r_1} of the centrode associated with the Z_5 rotor și radius of the inner rotor, R
x_1y_1	fixed reference system, with the origin at the rotation center of the Z_5 rotor, O_1 point
x_2y_2	fixed reference system, with the origin at the rotation center of the Z_4 rotor, O_2 point
X_1Y_1	mobile reference system, joined with the Z_5 rotor
X_2Y_2	mobile reference system, joined with the Z_4 rotor
R	the radius of the profile of inner rotor
Σ_1	the profile of the outer rotor
$R_{r_{\text{minim}}}$	minimum rolling radius
u	angular parameter that describes the Σ_1 profile
V	point on the rotor surface
Σ	the profile to be generated
$t-t$	tangent to the Σ_1 profile
$n-n$	normal to the Σ_1 profile, which passes through the O_1 origin
$X(u); Y(u)$	the parametric equations of the Σ_1 profile
Δ	the maximum distance between the current point on the Σ_1 profile și and the intersection point between the tangent to Σ_1 at the current point and the normal to Σ_1 , which passes through the origin of the reference system, O_1
Σ_2'	rolling profile
\bar{N}_Σ	normal to the Σ or Σ_1 profile
C_1	centrode associated with the Z_5 rotor
C_2	centrode associated with the Z_4 rotor
φ_1	the rotation angle of the reference system associated with the profile to be generated
φ_2	the movement parameter of the mobile reference system, joined with the tool profile, related to the φ_1 angle, by the rolling condition
P_v	virtual pole
\bar{r}_{P_v}	the position vector of the virtual pole

References

1. Gamez-Montero, P.J.; Codina, E.; Castilla, R. A Review of Gerotor Technology in Hydraulic Machines. *Energies* **2019**, *12*, 2423.
2. Vílchez, M.G. Design Tools Applied to a Trochoidal Gear Pump. Ph.D. Thesis, Universitat Politècnica de Catalunya (UPC), Barcelona, Spain, 2014.
3. De Martin, A. Development of a Novel Gerotor Pump for Lubrication Systems of Aeronautic Engines. Ph.D. Thesis, Politecnico di Torino, Turin, Italy, 2018.
4. Sang, X.; Zhou, X.; Liu, X. Numerical simulation of an inner engaging gerotor based on the optimization of inlet and outlet cavities. In Proceedings of the 5th International Conference on Advanced Design and Manufacturing Engineering, Shenzhen, China, 19–20 September 2015.
5. Demenego, A.; Vecchiato, D.; Litvin, F.L.; Nervegna, N.; Mancó, S. Design and simulation of meshing of a cycloidal pump. *Mech. Mach. Theory* **2002**, *37*, 311–332. [[CrossRef](#)]
6. Sliwinski, P.; Patrosz, P.; Bak, M.; Stosiak, M.; Urbanowicz, K.; Šukevičius, Š. Experimental Study of Flow Rate in Hydraulic Satellite Motor with the Rotating Case at a Low Constant Rotational Speed. In Proceedings of the International Conference Transbaltica XIII: Transportation Science and Technology, Vilnius, Lithuania, 15–16 September 2022.
7. Baroiu, N.; Moroşanu, G.A. *Hydraulic Drive Systems*; Academica Publishing House: Galati, Romania, 2022; ISBN 978-606-606-011-0.
8. Litvin, F.L. *Theory of Gearing*; Reference Publication 1212; NASA, Scientific and Technical Information Division: Washington, DC, USA, 1984.
9. Bonandrini, G.; Mimmi, G.; Rottenbacher, C. Theoretical analysis of internal epitrochoidal and hypotrochoidal machines. *Proc. Inst. Mech. Eng. C* **2009**, *223*, 1469–1480. [[CrossRef](#)]
10. De Martin, A.; Jacazio, G.; Sorli, M. Optimization of Gerotor Pumps with Asymmetric Profiles through an Evolutionary Strategy Algorithm. *Machines* **2019**, *7*, 17. [[CrossRef](#)]
11. Lee, S.H.; Kwak, H.S.; Han, G.B.; Kim, C. Design of Gerotor Oil Pump with 2-Expanded Cardioids Lobe Shape for Noise Reduction. *Energies* **2019**, *12*, 1126.
12. Kwak, H.-S.; Li, S.-H.; Kim, C. Performance improvement of an oil pump: Design of port assembled with gerotor (2-ellipses-combined lobe). *Int. J. Precis. Eng. Manuf.* **2016**, *17*, 1017–1024.
13. Gamez-Montero, P.J.; Castilla, R.; Codina, E.; Freire, J.; Morató, J.; Sanchez-Casas, E.; Flotats, I. GeroMAG: In-House Prototype of an Innovative Sealed, Compact and Non-Shaft-Driven Gerotor Pump with Magnetically-Driving Outer Rotor. *Energies* **2017**, *10*, 435.
14. Liu, H.; Lee, J.C. Development of Combined Trochoidal Profile of a Gerotor Pump. *J. Appl. Math. Phys.* **2016**, *4*, 28–32. [[CrossRef](#)]
15. Liu, H.; Lee, J.C.; Yoon, A.; Kim, S.T. Profile design and numerical calculation of instantaneous flow rate of a gerotor pump. *J. Appl. Math. Phys.* **2015**, *3*, 92–97.
16. Pellegrini, M.; Vacca, A.; Devendran, R.S. A Lumped Parameter Approach for Gerotor Pumps: Model Formulation and Experimental Validation. In Proceedings of the 10th International Fluid Power Conference, Dresden, Germany, 8–10 March 2016.
17. Arinaga, S.; Yoshida, K.; Takada, S.; Noda, M.; Inoue, K. The Latest Trends in Oil Pump Rotors for Automobiles. *SEI Tech. Rev.* **2016**, *82*, 59–65.
18. Mancò, S.; Nervegna, N.; Rundo, M. A contribution to the design of hydraulic lube pumps. *Int. J. Fluid Power* **2002**, *3*, 21–32.
19. Hussain, T.; Kumar, M.U.; Sarangi, N.; Sivaramakrishna, M. A Study on Effect of Operating Conditions on Gerotor Pump Performance. *Def. Sci. J.* **2022**, *72*, 146–150. [[CrossRef](#)]
20. Buono, D.; di Cola, F.D.S.; Senatore, A.; Frosina, E.; Buccilli, G.; Harrison, J. Modelling approach on a Gerotor pump working in cavitation conditions. *Energy Procedia* **2016**, *101*, 701–709.
21. Hsieh, C.F. Influence of gerotor performance in varied geometrical design parameters. *J. Mech. Des.* **2009**, *131*, 121008.
22. Kwon, S.M.; Kang, H.S.; Shin, J.-H. Rotor profile design in a hypogero rotor pump. *J. Mech. Sci. Technol.* **2010**, *23*, 3459–3470.
23. Kwon, S.M.; Kim, C.-H.; Shin, J.-H. Optimal rotor wear design in hypotrochoidal gear pump using genetic algorithm. *J. Cent. South Univ. Technol.* **2011**, *18*, 718–725.
24. Robison, A.; Vacca, A. Multi-objective optimization of circular-toothed gerotors for kinematics and wear by genetic algorithm. *Mech. Mach. Theory* **2018**, *128*, 150–168.
25. Strmčnik, E.; Majdič, F. The Pressure and Efficiency Characteristic of Hydraulic Gerotor Motor with the Floating Outer Ring. *Teh. Vjesn.* **2018**, *25*, 609–615.
26. Ivanović, L.; Stojanović, B.; Blagojević, J.; Bogdanović, G.; Marinković, A. Analysis of the Flow Rate and the Volumetric Efficiency of the Trochoidal Pump by Application of Taguchi Method. *Teh. Vjesn.* **2017**, *24*, 265–270.
27. Ippoliti, L.; Berten, O. Influence of inlet piping conditions on the performance of an aircraft engine lubrication system pump. In Proceedings of the 9th National Congress on Theoretical and Applied Mechanics, Brussels, Belgium, 9–11 May 2012.
28. Gamez-Montero, P.J.; Bernat-Maso, E. Taguchi techniques as an effective simulation-based strategy in the design of numerical simulations to assess contact stress in gerotor pumps. *Energies* **2022**, *15*, 7138.
29. Liu, Y.; Huang, L.; Xu, J.; Wang, Y. Analysis of flow field characteristics of cycloidal pump based on fluid solid interaction. *J. Braz. Soc. Mech. Sci. Eng.* **2021**, *43*, 465.
30. Joshi, R.H.; Patel, J.N.; Patwa, K.M.; Prajapati, S.U.; Banker, V.J.; Joshi, H.B. Design and development of rotor profile for screw pump—a review. *Int. J. Eng. Sci. Invent.* **2020**, *9*, 13–19.

31. Jeong, S.W.; Chung, W.J.; Kim, M.S.; Kim, M.S. Application of SolidWorks® & AMESim®—Based Updated Simulation Technique to Back-flow Analysis of Trochoid Hydraulic Pump for Lubrication. In Proceedings of the 2014 World Congress in Computer Science, Computer Engineering and Applied Computing, Las Vegas, NV, USA, 21–24 July 2014.
32. Yanhua, W.; Longlong, H.; Yong, L.; Jingsong, X. Comparative analysis of cycloid pump based on CFD and fluid structure interactions. *Adv. Mech. Eng.* **2020**, *12*, 1687814020973533.
33. Carconi, G.; D’Arcano, C.; Nervegna, N.; Rundo, M. Geometric Features of Gerotor Pumps: Analytic vs. CAD Methods. In Proceedings of the Bath/ASME Symposium on Fluid Power and Motion Control, Bath, UK, 12–14 September 2012.
34. Ivanović, L.T.; Veličković, S.N.; Stojanović, B.Ž.; Kandevo, M.; Jakimovska, K. The Selection of Optimal Parameters of Gerotor Pump by Application of Factorial Experimental Design. *FME Trans.* **2017**, *45*, 159–164. [[CrossRef](#)]
35. Kim, M.S.; Chung, W.J.; Jung, C.D.; Park, S.S.; Ahn, H.C.; Kim, H.C. On new methodology of AMESim® & CATIA® V5—Based cavitation simulation for flow rate control of trochoid hydraulic pump. In Proceedings of the 2011 International Conference on Mechatronics and Automation, Beijing, China, 7–10 August 2011.
36. Ivanović, L.; Rakic, B.; Stojanovic, B.; Matejic, M. Comparative analysis of analytical and numerical calculations of contact stresses at rotational elements of gerotor pumps. *Appl. Eng. Lett.* **2016**, *1*, 1–7.
37. Pareja-Corcho, J.; Moreno, A.; Simoes, B.; Pedrera-Busselo, A.; San-Jose, E.; Ruiz-Salguero, O.; Posada, J. A virtual prototype for fast design and visualization of gerotor pumps. *Appl. Sci.* **2021**, *11*, 1190. [[CrossRef](#)]
38. Akerdad, M.; Aboutajeddine, A.; Elmajdoubi, M. Reverse Engineering Canvas (REC): A Visual Tool for Supporting Reverse Engineering Activities. *Int. J. Interact. Des. Manuf.* **2021**, *15*, 249–257.
39. Zhang, E.; Chen, M.; Deng, B. Parametric Design on Internal Gear of Cycloid Gear Pump with NX10.0. *IOP Conf. Ser. Mater. Sci. Eng.* **2017**, *250*, 012068. [[CrossRef](#)]
40. Litvin, F.L.; Ignacio, G.P.; Alfonso, F. Generalized concept of meshing and contact of involute crossed helical gears and its application. *Elsevier Comput. Methods Appl. Mech. Eng.* **2005**, *194*, 3710–3745.
41. Baroiu, N.; Moroşanu, G.A.; Teodor, V.G.; Crăciun, R.S.; Păunoiu, V. Use of reverse engineering techniques for inspecting screws surfaces of a helical hydraulic pump. *Int. J. Mod. Manuf. Technol.* **2022**, *XIV*, 20–29. [[CrossRef](#)]
42. Berbinschi, S.; Teodor, V.; Baroiu, N.; Oancea, N. Profiling methodology for side mill tools for generation of helical compressor rotor using reverse engineering. *Ann. Dun. Jos Univ. of Galati.* **2011**, *V*, 111–116.
43. Baroiu, N.; Berbinschi, S.; Teodor, V.G.; Susac, F.; Oancea, N. The complementary graphical method used for profiling side mill for generation of helical surface. *IOP Conf. Ser. Mater. Sci. Eng.* **2017**, *227*, 012013.
44. Baroiu, N.; Moroşanu, G.A.; Teodor, V.G.; Oancea, N. Roller profiling for generating the screw of a pump with progressive cavities. *Inventions.* **2021**, *6*, 34. [[CrossRef](#)]
45. ATOS Core in Use with GOM Scan Software. Available online: <https://www.youtube.com/watch?v=751kz4SF7ME> (accessed on 15 March 2023).
46. Oprean, A.; Marin, V.; Dorin, A. *Accionări Hidraulice (Hydraulic Drives)*; Tehnică: Bucharest, Romania, 1976.
47. Galluzzi, R.; Xu, Y.; Amati, N.; Tonoli, A. Optimized design and characterization of motor-pump unit for energy-regenerative shock absorbers. *Appl. Energy* **2018**, *210*, 16–27.
48. Oancea, N. *Surfaces Generation through Winding*; Galati University Press: Galati, Romania, 2004; Volume I–III.
49. Costin, G.A.; Teodor, V.G.; Oancea, N. “Virtual Pole” method applied at the profiling of the rotary cutter tool for processing of ball screw. *IOP Conf. Ser. Mater. Sci. Eng.* **2020**, *916*, 012022.
50. Costin, G.A.; Teodor, V.G.; Oancea, N. The Virtual Pole method—An alternative method for profiling tools which generate by unwrapping. *Ann. of Dun. Jos Univ. Galati.* **2019**, *V*, 31–34.

Disclaimer/Publisher’s Note: The statements, opinions and data contained in all publications are solely those of the individual author(s) and contributor(s) and not of MDPI and/or the editor(s). MDPI and/or the editor(s) disclaim responsibility for any injury to people or property resulting from any ideas, methods, instructions or products referred to in the content.